# 6. Chapter 6 : Bottom-Electrode structures for the integration of SBT based capacitors into high density FRAMs.

## *6.1 Abstract*

The effect of various electrode materials on the ferroelectric properties of $SrBi_2Ta_2O_9$ (SBT) thin films has been investigated for non-volatile memory applications. Two sets of electrode structures, viz., Pt-Ir based and Pt-Rh based, were sputter deposited in-situ on Si substrates. SBT thin films were deposited on these electrodes using a metal-organic solution deposition technique followed by a post-deposition anneal at 750 $^0$C in oxygen atmosphere. Structural characterization revealed a polycrystalline nature with predominant perovskite phase in SBT thin films. Ferroelectric properties were studied in capacitor mode by depositing top electrodes, where the top electrode material is identical to that of bottom electrode. Extensive analysis of the ferroelectric properties signifying the important role played by the electrode material in establishing the device applicability is reported in this work.

### *6.2 Introduction*

Ferroelectric thin films have been investigated for their potential applications in memory devices[1-3], optical devices[4], piezoelectric devices[5], infrared detectors[6] and transistors[7]. Among them, thin films of lead zirconate titanate (PZT) and more recently, strontium bismuth tantalate (SBT) are most promising for nonvolatile memory applications. Presently, a one transistor-one capacitor (1T/1C) cell structure is being investigated for very large scale integration of ferroelectric memory devices[8]. In this design, polycrystalline silicon (polysilicon) is used as the plug to connect the transistor to the ferroelectric capacitor. This necessitates the bottom electrode of the capacitor be in direct electrical contact with polysilicon plug. Currently, platinum is being used as the bottom electrode for the capacitors. However, direct integration of platinum electrode based ferroelectric capacitors onto silicon cannot be achieved due to several problems which include interdiffusion[9], adhesion, and hillock formation. Among ferroelectric materials, SBT based capacitors have an additional advantage over their PZT counterparts owing to the fatigue-free nature of SBT and hence will be the focus of this study.

Taking into consideration all the above mentioned requirements, viz., diffusion barrier, highly conducting electrode, smooth morphology of the electrode on silicon, we have investigated several new electrode structures based on noble metal alloys and their oxides particularly Pt, Ir, Rh, their alloys and oxides. Although there have been several reports of electrode structures based on Pt, Ir, Ru and their oxides prior to this study,, most of them have been for PZT capacitors[10-12]. The few studies reported in literature, of

investigations on SBT based capacitors, showed good capacitor properties when measured only between the top and bottom electrodes[13]. The difference between their electrode structures and the ones reported here lies in the fact that the ferroelectric properties of SBT capacitors reported in this study were measured not only between the top and bottom electrodes but also between the highly doped poly Si substrate and the top electrode. This includes a thorough examination of the diffusion barrier properties of the electrode structures. In other words, we have attempted to develop electrode structures which also inherently act as diffusion barriers for Oxygen, Silicon and Bismuth. Fig. 6.1 shows the various SBT capacitor structures investigated in this study. All these structures were fabricated through in-situ deposition processes thereby avoiding the deposition of separate diffusion barrier and electrode layers.

The present studies were aimed particularly at investigating the diffusion barrier and electrode properties of SBT capacitors based on the electrode structures integrated directly onto silicon.

### *6.3 Experimental Procedure*

The substrates used for all the capacitor structures were n+(100) Si and n+polySi. The substrates were pre-cleaned using a $H_2SO_4$-$Cr_2O_3$ solution to remove the metallic impurities, followed by a hydrofluoric acid treatment to remove the native oxide on the surface. The different electrode structures investigated are shown in Figure. 6.1. All the electrode-structures were deposited using r.f.magnetron sputtering technique, using 99.99% pure 2 inch diameter, 0.125 inch thick targets, the details of which are given below.

#### 6.3.1 Bottom electrodes Deposition

(a) Pt-Ir based :

Ir, Pt and $IrO_2$ thin films in these electrode structures referred to as (a)1-3, in figure. 6.1, were deposited in-situ in a Cooke vacuum sputtering system. All the thin films were deposited at room temperature. For all the films, Argon was used as the sputter gas. For the Ir and Pt films were deposited at an argon partial pressure of 2 mtorr, while the $IrO_2$ layers were deposited in Ar+$O_2$ ambient at a total deposition pressure of 5mtorr. The deposition rates obtained for Pt, Ir and $IrO_2$ were 15, 10 and 8 nm/min respectively. All the as-deposited electrodes were annealed in vacuum oven at 450 $^oC$ for 30 min. before the SBT film deposition.

(b) Pt-Rh electrode structure:

PtRh and PtRhOx thin films were deposited in-situ in a Denton Vacuum sputter

system. A Pt-10%(weight)Rh target was used for sputtering. The substrate temperature was maintained constant at 450 $^{o}$C during the deposition. Pure Argon at 5 mtorr was used as the sputter gas and the deposition rate obtained was about 3 nm/min. PtRhOx was deposited in Ar+$O_2$ ambience similar to $IrO_2$, at a pressure of 7 mtorr and the deposition rate obtained was 5 nm/min.

6.3.2 SBT thin film deposition

Thin films of SBT were deposited on to the susbstrates using chemical solution deposition technique. The starting precursors were Sr-acetate, Ta-ethoxide and Bi-2ethyl-hexanoate, and acetic acid, 2-methoxyethanol and hexanoic acid were used as the respective solvents. The solution was coated on to substrates using spin coating, followed by a pyrolysis on a hot plate at 250 $^{o}$C. After the requisite thickness (about 300 nm) was obtained, the films were annealed at 750 $^{o}$C for one hour in oxygen environment in conventional annealing furnaces.

6.3.3 Top electrode deposition

The top electrodes for the capacitor structure were deposited using a shadow mask with the dot area of about $3.0x10^{-4}$ $cm^2$ using identical sputter deposition conditions as the bottom electrode.

6.3.4 Characterization

All the films were characterized for phase by X-ray diffraction using Cu-K□□from a Scintag 2000 diffractometer. The microstructure of the films was analyzed

using Atomic force microscopy (AFM) from Digital Instruments. Ferroelectric properties such as hysteresis, leakage current and fatigue were measured bot between the top and the bottom electrodes as well as between the n+poly Si and the top electrode using a RT66A from Radiant Technologies. The diffusion barrier properties of the electrode structures were studied using Auger electron spectroscopy.

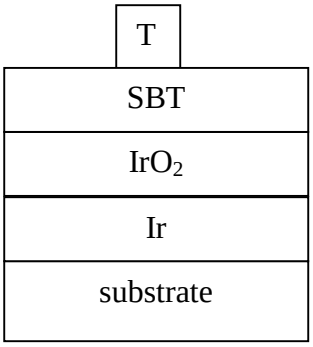


(a) - 1

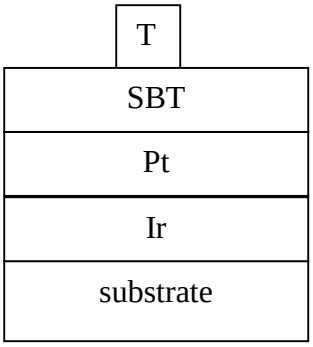


(a) - 2

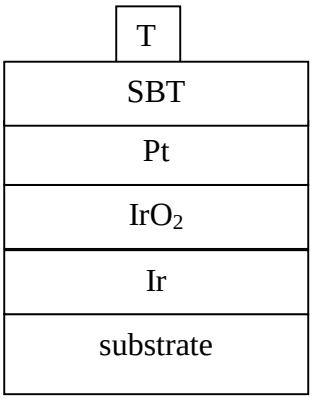


(a) - 3

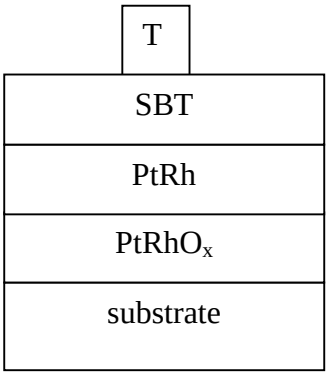


(b)

Fig. 6.1 Different electrode structures investigated in this study. (a) 1, 2, 3 Pt-Ir based and (b) Pt-Rh based. TE stands for the top electrode which was identical to the bottom electrode structure.

### *6.4 Results and Discussion*

X-ray diffraction studies showed that the Ir films were crystalline as deposited, while the $IrO_2$ thin films were amorphous. Moreover, the oxygen content in the $IrO_2$ thin films was found to be greater than 2. In order to reduce the oxygen content to the stoichiometric value, the films were annealed in vacuum upon which the excess oxygen was lost. All the electrodes showed a smooth morphology as measured using AFM. SBT was deposited on top of these electrodes and the phase, morphology examined. Then dots of area around $3.0x10^{-4}cm^2$ were sputter deposited as top electrodes on the SBT films to complete the capacitor structure. Ferroelectric properties were measured both between the top and bottom electrodes as well as between the top electrode and the highly doped conducting Si substrate using a silver paint. All these results will be discussed in the following sections.

**(A) Phase and morphological characteristics**

Figure 6.2 shows the X-ray diffraction patterns of SBT thin films on both Pt-Ir based as well as PtRhOx electrode structures. It can be seen that SBT crystallizes in randomly oriented fashion on all the electrodes. From figure 6.2 (a), on the capacitor structure TE | SBT | IrOx | Ir | Si, Iridium silicide and Bismuth silicate also are formed along with SBT phase. This shows that iridium is not stable even in the oxide form at the processing temperatures of SBT resulting in the formation of iridium silicide. Also, the formation of bismuth silicate peak at a 2-theta value of 53 indicates the diffusion of silicon into the ferroelectric or the diffusion of bismuth into the

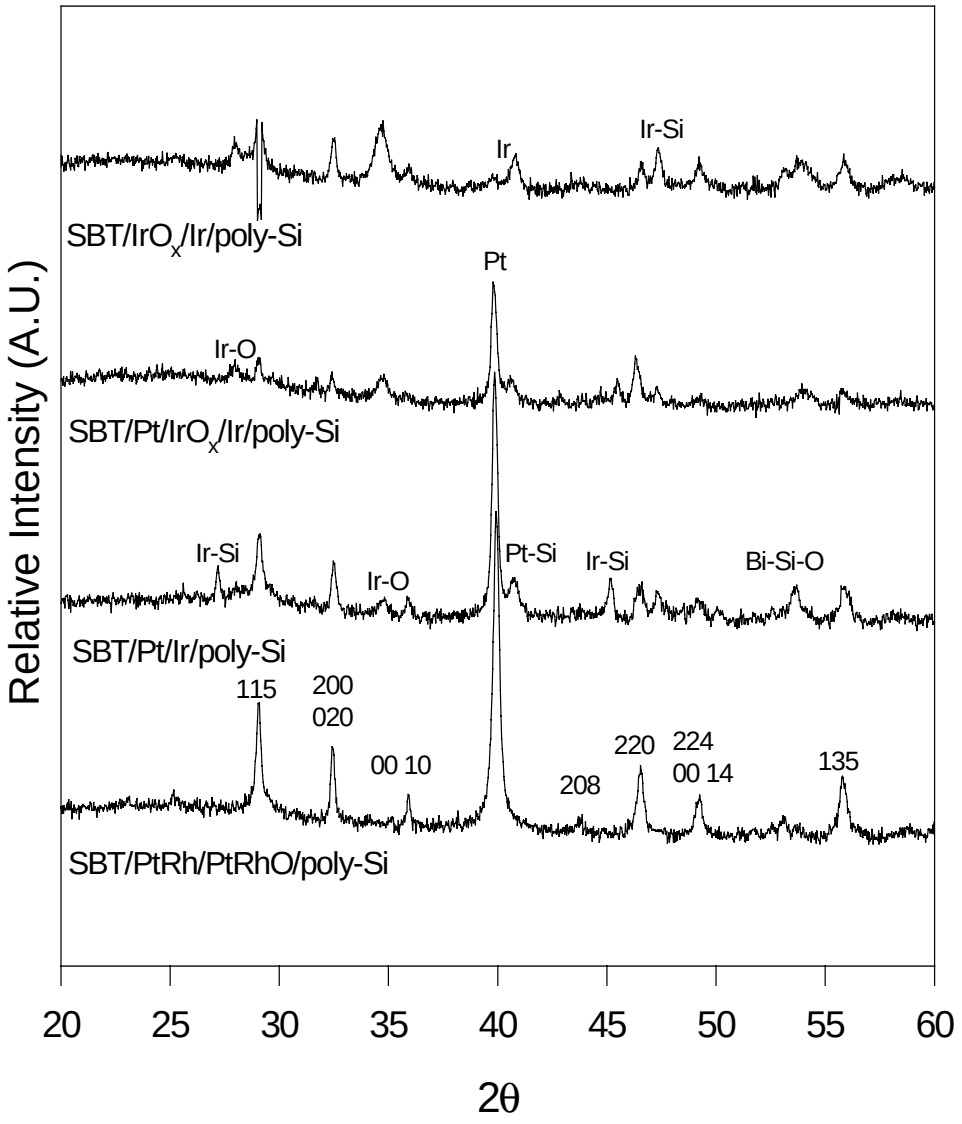


Fig 6.2 XRD patterns of SBT thin films deposited on Pt-Ir based electrode structures and PtRh based electrode structure.

substrate. Either way, this indicates that the structure IrOx|Ir does not act as very good diffusion barrier for integration of SBT – PtIrOx capacitor structure on to the silicon plug. Similar is the case with TE | SBT | Pt | IrOx | Ir | n+poly Si and TE | SBT | Pt | Ir | n+poly Si capacitor structures. However, from figure 6.2(b), the TE | SBT | PtRh | PtRhOx | n+poly Si capacitor structure showed no extraneous peaks. The XRD pattern shows a well crystallized SBT phase on these electrode structures indicating no second phase formation. The absolute intensity of the peaks also shows the maximum on PtRhOx electrode structures indicating maximum size of the crystallites formed.

In order to confirm the observations from the x-ray diffraction patterns, AFM studies were performed on the SBT thin films deposited on all the electrode structures. Figure 6.3 shows the atomic force microscopy micrographs of SBT thin films on the proposed electrode structures. Although the secondary phases as seen from the XRD studies could not be detected from AFM, it is clear that the grain size of SBT thin films is different on different electrode structures although the processing temperature was maintained constant at 750 $^{o}$C. Among all the electrode structures investigated in this study, the grain size of SBT thin films on PtRhOx | PtRh structures proved to be the maximum.

**(B) Diffusion barrier properties**

Along with the grain size, it is important that these structures act as good diffusion barriers for silicon, oxygen and bismuth. Therefore, a detailed analysis of the diffusion barrier properties of the electrode structures was performed using Auger electron spectroscopy. Figure 6.4 shows the auger electron spectra of SBT on Pt | Ir | poly Si and PtRh | PtRhOx | poly Si

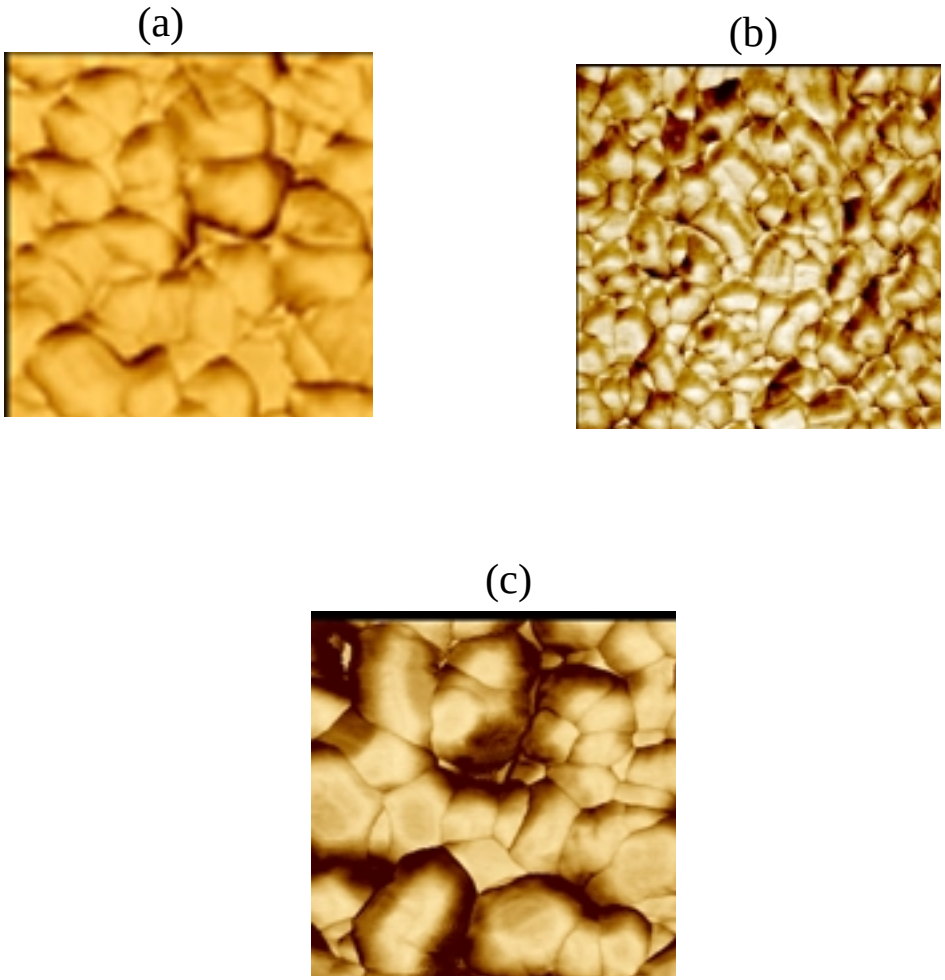


Fig. 6.3. AFM micrographs (1 μm x 1 μm) of SBT thin films on (a) $IrO_x$/Ir/n+poly-Si, (b) pt/Ir/n+poly-Si and (c) PtRh/$PtRhO_x$/n+poly-Si electrode structures.

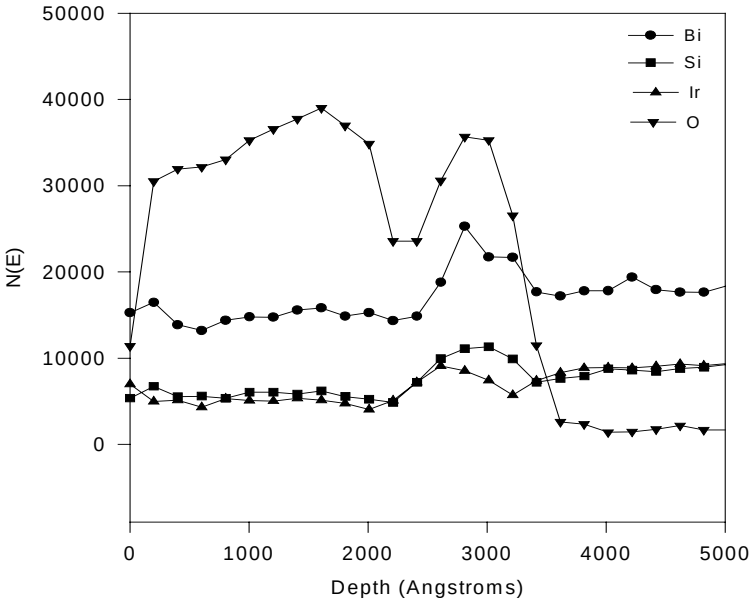


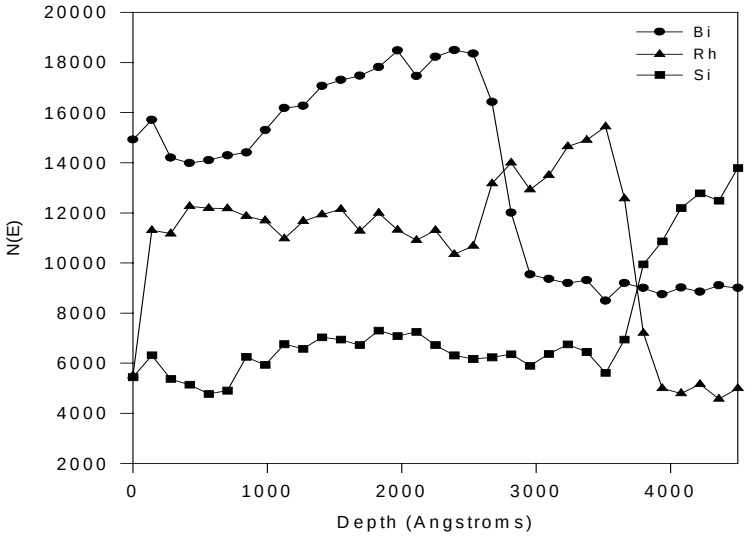


Fig. 6.4 Auger electron spectra of SBT thin films on (a) Pt/Ir/poly-Si and (b) PtRh/PtRhOx/poly-Si electrode structures

structures. It was observed that the other Pt-Ir based electrode structures also showed a similar behavior and hence, will not be discussed here. From figure 4(a), it can be seen that Si, O and Bi ions diffused into the electrode structure, indicating instability of the barrier at the processing temperatures of PZT.

(C) Ferroelectric properties

Table 6.1 shows the results from the measurements of ferroelectric properties on various electrode structures. It was observed that the TE | SBT | IrOx | Ir | poly Si capacitors were short to begin with and did not show any ferroelectric properties indicating its instability. Hence, these results are not included in the table. The TE | SBT | Pt | Ir showed good ferroelectric properties, but the properties when tested between the poly Si plug and the top electrode showed different values of remnant polarization, leakage current density and fatigue. Although the exact reason for this difference is not known at present, it could speculatively be attributed to the inferior diffusion barrier properties of the structure. On the other hand, the ferroelectric properties of the capacitors based on the PtRhOx | PtRh electrode structures showed no measurable difference when tested between the top and bottom electrode or between the poly Si plug and the top electrode. This is also evidence, although indirect, that the PtRhOx structure acts as an excellent diffusion barrier. For comparison purposes, the SBT capacitors based on just Pt have been included in the figure. This corroborates the results indicated from auger depth profiles shown in figure 6.4. The same fact is further elucidated in figure 6.5 which compares the ferroelectric hysteresis behavior of the capacitors. Capacitors based on PtRh electrode structure exhibit excellent ferroelectric properties along with very

Table 6.1 Summary of ferroelectric properties of the SBT capacitors deposited on various electrodes.

| **Capacitor Structure** | **$P_r$ ($\mu C/cm^2$)** | **$E_c$ (kV/cm)** | **$I_L$ (100kV/cm)-$A/cm^2$** | **Fatigue (after $10^{11}$ cycles)** |
|---|---|---|---|---|
| Pt/SBT/Pt | 6.5 | 35 | $10^{-10}$ | <1% |
| Ir/Pt/SBT/Pt/Ir | 5.5 | 45 | $10^{-7}$ | <5% |
| Ir/Pt/SBT/Pt/Ir/Si | 4.3 | 50 | $10^{-8}$ | <5% |
| Ir/$IrO_x$/SBT/$IrO_x$/Ir | - | - | $10^{-4}$ | - |
| Ir/$IrO_x$/SBT/$IrO_x$/Ir/Si | - | - | $10^{-4}$ | - |
| TE/SBT/PtRh/PtRh$O_x$ | 6.3 | 40 | $10^{-10}$ | <1% |
| TE/SBT/PtRh/PtRh$O_x$/Si | 6.3 | 40 | $10^{-10}$ | <1% |

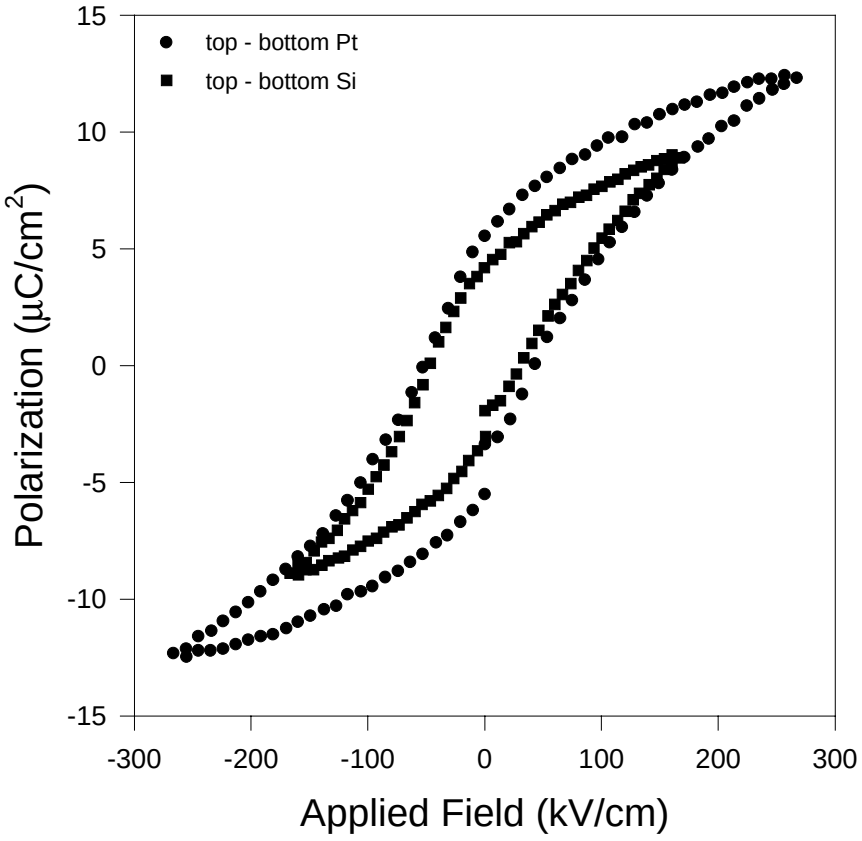


Fig. 6.5(a) Hysteresis behavior of capacitors Top-electrode/SBT/Pt/Ir/n+poly-Si and Top-electrode/SBT/Pt/Ir structure.

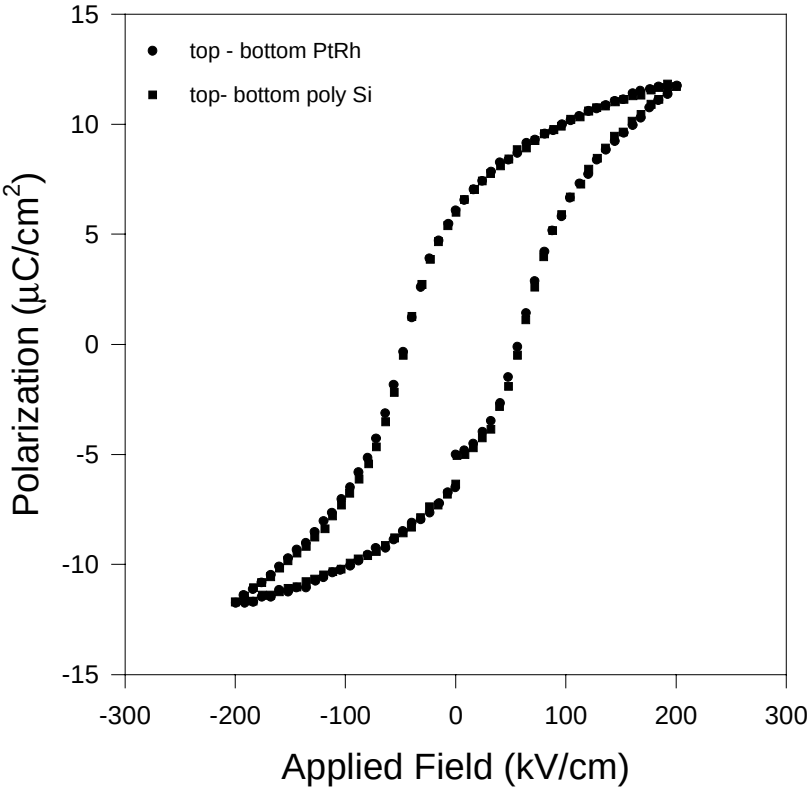


Fig. 6.5(b) Hysteresis behavior of capacitors Top-electrode/SBT/PtRh/PtRhOx/n+poly-Si and Top-electrode/SBT/PtRh/PtRhOx structure.

good diffusion barrier properties for SBT thin films.

### *6.5 Conclusions*

Several Pt-Ir and Pt-Rh based electrode structures have been investigated for direct integration of SBT capacitors on to the polySi plug in FRAM devices. SBT thin films have been deposited using sol-gel technique on to these Pt-Rh and Pt-Ir based electrode structures. The diffusion barrier properties of these electrode structures have been analyzed using Auger Electron Spectroscopy. The electrode characteristics were examined not only between the top and bottom electrodes but also between the conducting substrate and the top electrode. Auger studies indicated that the Pt-Ir based electrode structures do not act as barriers for the diffusion of Si, O and Bi ions into the electrode. Consequently, the ferroelectric properties were inferior to those on conventional Pt electrodes. However, PtRhOx based electrode structure acts not only as an excellent diffusion barrier but also exhibited ferroelectric properties comparable to those on Pt even when measured between the top electrode and the conducting polySi substrate. In summary, we have attempted to integrate SBT capacitors on top of the polySi plug in FRAM and PtRhOx based electrode structures show great potential in these applications.

***References***


1. J.F.Scott and C.A. Araujo, Science, 246 (1989) 1400.
2. R. Moazami, C. Hu and W. H. Shepherd, IEEE Trans. Electron Devices, 39 (1992), 2044.
3. J. T. Evans and R. Womack, IEEE Solid-State Circuit, 23 (1988), 1171.
4. K.D. Preston and G. H. Haertling, Appl. Phys. Lett., 60 (1992), 2831.
5. M. Okuyama and Y. Hamakawa, Ferroelectrics, 63 (1985), 243.
6. M. Okuyama, H. Seto, M. Kojima, Y. Matsui and Y. Hamakawa, Jpn. J. Appl. Phys., 22, Suppl. 22-1 (1983), 465.
7. V. I. Petrovsky, A. S. Sigov and K. A. Vorotilov, Integrated Ferroelectrics, 3 (1993), 59.
8. S. Yokoyama et al, Jpn. J. Appl. Phy.(I), 34, #2 (1995), 767.
9. K. Shoji, et al, VLSI Tech. Symp. Digest of Technical papers, 28 (1996).
10. K.Amanuma, et al, Ferroelectric Thin Films IV, (Materials Research Symposium, Pittsburgh) 1995, 21.
11. T. Nakamura, et al, Appl. Phys. Lett., 65 (12) 1994 p1522.
12. Y. C. Jeon, et al, Appl. Phys. Lett., 71 (4) 1997 p467.
13. Y. Nakao, et al, Jpn. J. Appl. Phys., V33, (1994) part I, No. 9B, B5265.